

# Study of Ionic Currents across a Model Membrane Channel Using Brownian Dynamics

Shin-Ho Chung,\* Matthew Hoyles,\*\* Toby Allen,\* and Serdar Kuyucak#

\*Protein Dynamics Unit, Department of Chemistry, and \*\*Department of Theoretical Physics, Research School of Physical Sciences, Australian National University, Canberra, A.C.T. 0200, Australia

**ABSTRACT** Brownian dynamics simulations have been carried out to study ionic currents flowing across a model membrane channel under various conditions. The model channel we use has a cylindrical transmembrane segment that is joined to a catenary vestibule at each side. Two cylindrical reservoirs connected to the channel contain a fixed number of sodium and chloride ions. Under a driving force of 100 mV, the channel is virtually impermeable to sodium ions, owing to the repulsive dielectric force presented to ions by the vestibular wall. When two rings of dipoles, with their negative poles facing the pore lumen, are placed just above and below the constricted channel segment, sodium ions cross the channel. The conductance increases with increasing dipole strength and reaches its maximum rapidly; a further increase in dipole strength does not increase the channel conductance further. When only those ions that acquire a kinetic energy large enough to surmount a barrier are allowed to enter the narrow transmembrane segment, the channel conductance decreases monotonically with the barrier height. This barrier represents those interactions between an ion, water molecules, and the protein wall in the transmembrane segment that are not treated explicitly in the simulation. The conductance obtained from simulations closely matches that obtained from ACh channels when a step potential barrier of  $2\text{--}3 kT_r$  is placed at the channel neck. The current-voltage relationship obtained with symmetrical solutions is ohmic in the absence of a barrier. The current-voltage curve becomes nonlinear when the  $3 kT_r$  barrier is in place. With asymmetrical solutions, the relationship approximates the Goldman equation, with the reversal potential close to that predicted by the Nernst equation. The conductance first increases linearly with concentration and then begins to rise at a slower rate with higher ionic concentration. We discuss the implications of these findings for the transport of ions across the membrane and the structure of ion channels.

## INTRODUCTION

Theoretical studies of the biological ion channel have been hampered by a lack of detailed structural knowledge. The exact shape of any biological channel, either ligand-gated or voltage-activated, is unknown, as are the positions, densities, and types of dipoles and charge moieties on the protein wall. These details are needed to compute the intermolecular potential operating between water molecules, ions, and the protein wall, which is the essential ingredient for microscopic studies of channels using molecular dynamics. Even if such information were available, it would not be feasible at present to carry out molecular dynamics calculations for all of the water molecules and ions in a biological channel and its surroundings for a period long enough to deduce any of its macroscopically observable properties. For these and other reasons, it has not been possible to compare the results obtained from microscopic models with the real data obtained from patch-clamp recordings. There is a need to develop models that can relate the structural parameters of channels to experimental measurements and to build a theoretical framework that interlaces all of the

disparate sets of observations into a connected whole. The theoretical model described in this paper was produced in the hope of furthering this aim.

It is possible to make the computations tractable by making several simplifications of and idealizations about the channel and electrolyte solutions, and to examine the magnitude of currents flowing through the model conduit under various conditions, using Brownian dynamics simulations (Cooper et al., 1985). Brownian dynamics provides one of the simplest methods for following the trajectories of idealized particles in a fluid interacting with a dielectric boundary. Here the water is treated as a continuum, and the motions of individual ions are assumed to be governed by electrostatic forces emanating from other ions, fixed charges in the proteins, the applied electric field and the dielectric boundary. The effects of solvation and the structure of water are taken into account by frictional and random forces acting on ions. Brownian dynamics simulations have already been fruitfully utilized to investigate the movement of ions across a model cylindrical tube (Jakobsson and Chiu, 1987; Chiu and Jakobsson, 1989; Bek and Jakobsson, 1994) and a toroidal channel (Li et al., 1998). With these simulations, it was possible to capture some of the salient features of biological ion channels and reveal the importance of the vestibules in influencing the permeability properties of ions through the pore.

To deduce the conductance of a model channel with Brownian dynamics simulations, the number of ions placed in the reservoirs that mimic the extracellular and intracel-

Received for publication 5 December 1997 and in final form 5 May 1998.

Address reprint requests to Dr. S. H. Chung, Protein Dynamics Unit, Department of Chemistry, Australian National University, Canberra, A.C.T. 0200, Australia. Tel.: 61-2-6249-2024; Fax: 61-2-6247-2792. E-mail: shin-ho.chung@anu.edu.au.

© 1998 by the Biophysical Society

0006-3495/98/08/793/17 \$2.00

ular media must be relatively large, and the simulation period needs to be sufficiently long that reliable statistics for currents flowing across the channel can be collected. With this requirement in mind, we have devised a method of reducing the amount of computational effort involved in simulating a system of charged particles interacting with a protein wall. Instead of computing the force acting on an ion at each position and at each time step, we precalculated the values of the electric potential and field for a grid of positions and stored them in a set of lookup tables. Using a multidimensional interpolation algorithm (Press et al., 1989), the field and potential experienced by an ion at any position could be deduced from the information stored in the lookup tables. Using this method, we were able to study ionic currents flowing across a realistic model channel under various conditions.

Brownian dynamics simulations do not adequately capture the transport process of ions in the narrow, constricted channel region. This is because water is treated as continuum, ions are idealized as point particles, and the protein wall is represented as a structureless, rigid, and smooth dielectric surface. In this narrow cylindrical region, polar groups on the protein wall are likely to interact with the primary or secondary hydration shell of an ion as it drifts across the conduit, possibly replacing several water molecules in the shell and forming temporary hydrogen bonds with the ion. Elucidation of the permeation processes taking place in the transmembrane segment will require molecular dynamics calculations, such as the ones carried out for the gramicidin pore (Roux and Karplus, 1991a). In the absence of a detailed knowledge of the location and types of polar groups lining the channel wall and the precise geometry of the transmembrane segment, we have represented the intermolecular interactions taking place between ions, water molecules, and the protein wall in this region as a step potential barrier of variable height. The barrier is constructed such that it rises gently to the desired height in 1 Å, and its first and second derivative are zero at the end points. Thus the energy must be paid to enter the neck and is returned when the ion exits.

Here we describe a model channel and report the results of Brownian dynamics calculations aimed at elucidating the permeation of ions through it. The shape of the channel is made approximately the same as that of the ACh channel (Toyoshima and Unwin, 1988), and cylindrical reservoirs containing sodium and chloride ions are placed at each end of the channel. We show that by placing an appropriate strength of dipoles in the channel wall and erecting a small energy barrier at the entrance of the narrow transmembrane segment, we can replicate some of the macroscopically observable properties of biological ion channels. Among these are the channel conductance, an ohmic current-voltage relationship, inward rectification as predicted by the Goldman equation, and the conductance-concentration relationship.

## METHODS

### The channel model

There are two major impediments to formulating a microscopic model of membrane ion channels and simulating molecular trajectories of idealized particles interacting with the protein boundary. First, the description of the protein wall forming a narrow cavity is relatively incomplete. For example, the precise shape, and the number, magnitude, and location of dipoles or charge moieties on the protein wall of biological ion channels are unknown. Second, even with the most advanced computer currently available, it is not feasible to simulate motion of all water molecules and ions in a channel and surroundings for a period long enough to measure conductance. To study the permeation of ions through a biological channel, we need to devise an idealized model channel and then make several simplifying assumptions about the intermolecular potential that operates between particles in the assembly. We therefore make the following simplifications and idealizations about our model channel to enable us to simulate current flow across the channel under various conditions.

#### *Shape of the channel*

A catenary channel was generated by rotating the closed curve shown in Fig. 1 *A* around the axis of symmetry ( $z$  axis). The vestibule of the channel, whose shape is similar to that visible in the electron microscope picture of the acetylcholine channel (Toyoshima and Unwin, 1988), was generated by a hyperbolic cosine function,  $z = a \cosh x/a$ , where  $a = 4.87$  Å. The radius of the entrance of the vestibule was fixed at 13 Å. Two identical vestibules were connected with a cylindrical transmembrane region of length 10 Å and radius 4 Å. A cross section of the model channel, the total interior volume of which was  $2.16 \times 10^{-26}$  m<sup>3</sup>, is illustrated in Fig. 1 *B*. We assumed, for convenience, that the two vestibules are identical in size, although the image of the channel produced by Toyoshima and Unwin (1988) shows that the extracellular vestibule is larger than the intracellular vestibule.

#### *Dipoles in the protein wall*

To investigate how the permeation of ions across the channel is influenced by the presence and absence of dipoles in the protein wall, we placed in some simulations a set of four dipoles inside the protein boundary at  $z = 5$  Å and another set of four dipoles at  $z = -5$  Å. Their orientations were perpendicular to the central axis of the lumen ( $z$  axis). For each dipole, the negative pole, placed 2 Å inside the water-protein boundary, was separated from the positive pole by 5 Å. Thus if 5/16 of an elementary charge was placed on each pole, then the total moments of four such dipoles would be  $100 \times 10^{-30}$  Coulomb-meter. The same configuration of dipoles was used in all of the simulations, giving rise to an

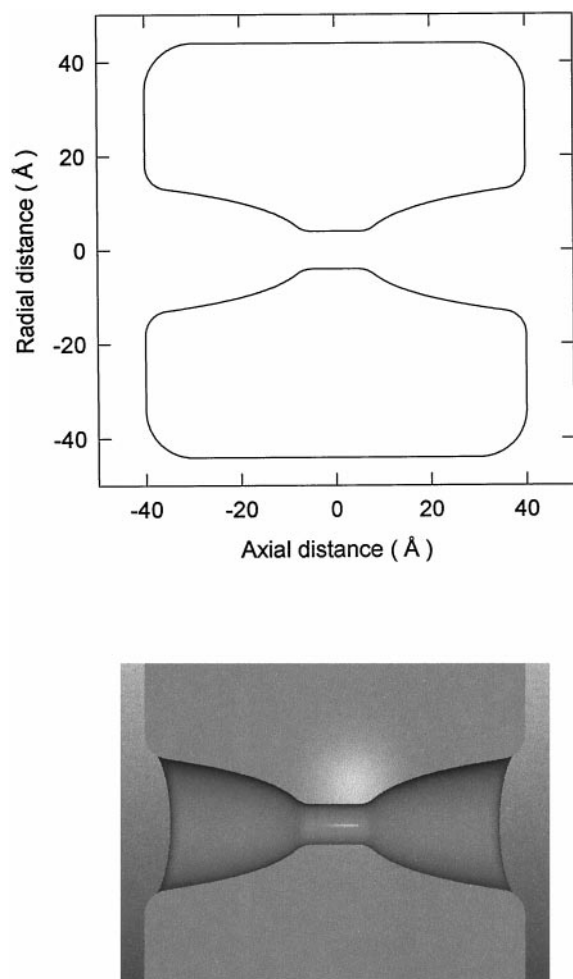


FIGURE 1 Idealized biological ion channel. A model channel with two catenary vestibules was generated by rotating the closed curves outlined in *A* along the symmetry  $z$  axis (*horizontal line*) by  $180^\circ$ . A transverse section of the channel so generated is shown in *B*. To approximate the shape of the acetylcholine receptor channel, vestibules at each side of the membrane were constructed by using a hyperbolic cosine function,  $z = a \cosh x/a$ , where  $a = 4.87 \text{ \AA}$ . The radius of the entrance of the vestibule was fixed at  $13 \text{ \AA}$ , and the cylindrical transmembrane segment had a radius of  $4 \text{ \AA}$ . Each cylindrical reservoir,  $60 \text{ \AA}$  in diameter and  $22 \text{ \AA}$  in height, contained a fixed number of sodium and chloride ions. Unless stated otherwise, the ionic concentration in the volume composed of the channel vestibules and the reservoirs was  $300 \text{ mM}$ . The cylindrical reservoir had a glass boundary, in that an ion moving out of the boundary was reflected back into the reservoir.

attractive potential for sodium ions and a repulsive potential for chloride ions in the channel. These fixed charges represent the charged side chains thought to form a ring around the entrance of the constricted region (Unwin, 1989), and their nearby counter-charges. For convenience, we adjust the amount of charge rather than the number or positions of the charges, but in reality the side chains of charged amino acid residues would have one electron charge each if they are fully ionized or unprotonated at neutral pH. Polar groups located in the transmembrane segment of the channel that may rotate in and out form temporary hydrogen bonds with

an ion navigating across it, as found in gramicidin A pores, are not explicitly modeled in this study.

#### *Energy barrier to penetrating the transmembrane segment*

An ion in the vestibule needs to surmount an energy barrier to traverse the narrow, constricted segment of the channel. The presence of such an additional energy barrier in the gramicidin pore has been revealed by molecular dynamics calculations. Additional evidence is provided by the conductance-temperature curves measured from biological ion channels, which are always steeper than the conductivity-temperature curve of bulk electrolyte solutions. This steeper rise in the channel conductance with temperature is interpreted as being due to the presence of a dynamic barrier that ions need to overcome (Kuyucak and Chung, 1994; Chung and Kuyucak, 1995). Intuitively, this barrier arises from the interactions between the protein wall and the hydrated ion as the ion negotiates its way into the narrow, cylindrical transmembrane pore. To enter the narrow segment, the hydration shell of an ion needs to be rearranged, or some of the water molecules in the primary or secondary hydration shell need to be substituted with polar groups on the protein wall. To rearrange the ion-water geometry requires an additional energy, and the ion can surmount such a barrier only when it gains a sufficient kinetic energy. To mimic a barrier present in the ion channel, we placed in some simulations a potential step near the constricted segment of the channel. The method we used for implementing such a potential barrier in the Brownian dynamics algorithm is detailed in the Methods.

#### *Water as a continuum*

We treat the water as a continuum in which the ions move under the influence of electrostatic forces and random collisions. In the constricted region of the channel, where the radius is  $\sim 4 \text{ \AA}$ , the representation of water molecules as a continuous dielectric medium is a poor approximation. The addition of energy barriers to the model is an attempt to compensate for this difficulty. We represent the water-protein interface as a single sharp and rigid boundary between dielectrics. In reality, however, the channel wall is not made of a structureless dielectric material. Instead, its surface is likely to be lined with hydrophilic and polar side chains, which will restrict the ability of water molecules to align with the electric field. The interface could be more accurately represented as a region of intermediate dielectric constant. Because the use of a single boundary does not introduce significant error, as has been shown elsewhere (Hoyle et al., 1996), we adopt the simpler model. The polar groups and ordered water at the interface are not explicitly included in our model, being represented by the dielectric boundary.

### Applied electric field

A potential difference across a lipid membrane is produced by a surface charge density on each side of the membrane. In microscopic terms, the surface charge density is a cloud of unpaired ions on either side of the membrane. Because these clouds are too diffuse to be explicitly included in our simulation, we apply an external electric field  $\mathcal{E}$  of a constant strength to represent the average effect of the ionic clouds. In the absence of any dielectric boundary, the potential difference across a channel with the length  $d$  is  $\mathcal{E}d$ . The presence of a dielectric boundary, however, severely distorts the field, enhancing it in the transmembrane segment and attenuating it in the vestibule (Kuyucak et al., 1998). Thus the precise potential difference will depend on the selected reference points at the two sides of the catenary channel. For simplicity, we apply a field strength of  $10^7$  V  $m^{-1}$  and refer to it as an applied potential of 100 mV.

### Brownian dynamics

The trajectories of ions drifting across the channel under the influence of a driving force while executing random thermal motion were followed with Brownian dynamics simulations. A detailed account of the theory underlying Brownian dynamics calculations is given elsewhere (Li et al., 1998). Briefly, the computational method traces the motion of the  $i$ th ion with mass  $m_i$  and charge  $q_i$  with the Langevin equation:

$$m_i \frac{dv_i}{dt} = -m_i \gamma_i v_i + F_R(t) + q_i \mathcal{E}_i. \quad (1)$$

The first term on the right-hand side of Eq. 1 corresponds to an average frictional force with the friction coefficient given by  $m_i \gamma_i$ , where  $1/\gamma_i$  is the relaxation time constant of the system. The second term,  $F_R(t)$ , represents the random part of the collisions and rapidly fluctuates around a zero mean. The frictional and random forces in Eq. 1, which together describe the effects of collisions with the surrounding water molecules, are connected through the fluctuation-dissipation theorem (Reif, 1965), which relates the friction coefficient to the autocorrelation function of the random force,

$$m_i \gamma_i = \frac{1}{2kT} \int_{-\infty}^{\infty} \langle F_R(0)F_R(t) \rangle dt, \quad (2)$$

where  $k$ ,  $T$ , and  $m$  are the Boltzmann constant, the temperature in degrees Kelvin, and the mass of the ion, respectively, and angle brackets denote ensemble averages. Finally,  $\mathcal{E}_i$  in Eq. 1 denotes the total electric field at the position of the ion arising from 1) other ions, 2) fixed charges in the protein, 3) membrane potential, and 4) induced surface charges on the water-protein boundary. This term in Eq. 1 is computed by solving Poisson's equation. Note that in three dimensions, Eq. 1 has to be solved for each Cartesian component ( $x$ ,  $y$ ,  $z$ ) of the velocity.

### Computational steps

The Brownian dynamics algorithm we used for solving the Langevin equation is that devised by van Gunsteren and Berendsen (van Gunsteren and Berendsen, 1982; van Gunsteren et al., 1981). That the behavior of the interacting ions deduced from simulations using this algorithm accords with the physical reality is detailed elsewhere (see Li et al., 1998). To compute the positions and velocities of ions at discrete time steps of  $\Delta t$ , the algorithm takes the following computational steps:

Step 1. Compute the magnitude of the electric force  $F(t) = q_i \mathcal{E}_i$  acting on each ion at time  $t_n$  and calculate its derivative  $[F(t_n) - F(t_n - 1)]/\Delta t$ .

Step 2. Compute a net stochastic force impinging on each ion over the time period of  $\Delta t$  from a sampled value of  $F_R(t)$ .

Step 3. Determine the position of each ion at time  $t_n + \Delta t$  and its velocity at time  $t_n$  by substituting  $F(t_n)$ , its derivative  $F'(t_n)$  and  $F_R(t)$  into the solutions of the Langevin equation (equations 2.6 and 2.22 of van Gunsteren and Berendsen, 1982).

Step 4. Repeat the above steps for the desired number of simulation steps.

Throughout, we used the time step of  $\Delta t = 100$  fs, except when an ion entered one of the two imaginary bands placed around the rising and falling edges of the step energy barrier (see the following section).

### Implementation of a step potential barrier in the algorithm

The use of a long time step causes a problem in implementing potential barriers and steps in Brownian dynamics as short-range forces. In our simulations, the Brownian dynamics algorithm operates predominantly in the diffusive regime. In other words, random forces are far more important than the velocity on the previous step in determining the anion's new velocity and position. The algorithm devised by van Gunsteren and Berendsen (1982) uses the factors  $[\exp(-\gamma\Delta t)]$  and  $[1 - \exp(-\gamma\Delta t)]$  to switch between kinetic and diffusive regions. With the long time step that we use ( $\Delta t = 100$  fs),

$$1 - \exp(-\gamma_{Na}\Delta t) = 0.9997,$$

$$1 - \exp(-\gamma_{Cl}\Delta t) = 0.9666.$$

Thus for chloride ions only 3% of the previous velocity remains after one time step, whereas the motion of sodium ions is in effect purely diffusive, with no velocity correlation between steps. Because an ion can move a large fraction of the barrier width in a single time step ( $\sim 0.3$  Å on average), the effect of the barrier force on the ion's motion will not be accurately integrated. Moreover, in the diffusive regime, external forces cause only an average drift velocity that does not move the ion far in a single time step. For example, a repulsive force of  $120 \times 10^{-12}$  N ( $3 kT_r$  over 1

Å) produces a drift velocity of  $39 \text{ ms}^{-1}$  for sodium and a displacement of  $0.04 \text{ Å}$  in one time step. This is only  $1/7$  of the average random displacement in one time step—an ion can diffuse right through a potential barrier before the barrier force has time to act.

To obviate these problems, we used two different time steps: a short time step of  $1 \text{ fs}$  when an ion was in the process of climbing or descending the barrier, and a long time step of  $100 \text{ fs}$  otherwise. A smooth potential barrier of height  $V_B$  was erected at  $z = \pm 10 \text{ Å}$  ( $5 \text{ Å}$  from the entrance of the cylindrical segment), with the profiles at the ends as

$$U(s) = V_B(10s^3 - 15s^4 + 6s^5), \quad (3)$$

where

$$s = \frac{z - z_b}{\Delta z} + \frac{1}{2}. \quad (4)$$

Here  $z_b = \pm 10 \text{ Å}$  is the location of the center of the profile, and  $\Delta z = 1 \text{ Å}$  is the width of the profile. The potential profile  $U(s)$  is chosen such that it rises from zero at  $z = \pm 10.5$  to  $V_B$  at  $z = \pm 9.5$ , and the first and second derivatives of  $U(s)$  vanish at  $z = \pm 9.5$  and  $z = \pm 10.5$ . The force due to the barrier is obtained by differentiating Eq. 3.

We included a safety distance of  $0.5 \text{ Å}$  in the potential profile. Thus, whenever ions were in the band of  $z = 9$  to  $11 \text{ Å}$  or  $z = -9$  to  $-11 \text{ Å}$ , we switched from long time steps to an equivalent sequence of short time steps for those ions. Trajectories of ions in these bands were determined by a sequence of  $100$  short time steps for the subsequent  $100 \text{ fs}$ . In the meantime, all of the other ions were simulated for a single long time step in the normal way. The long-range (electrostatic) forces on the ion were calculated at the start of the sequence of  $100$  short steps and held constant thereafter. Similarly, reflection from the boundary walls was done once at the end of the sequence of short steps. The force from the barrier, however, was recalculated for each short step, thus ensuring that the effect of the barrier on the ion's motion would be accurately simulated.

### Lookup tables for the electric field and potential

To reduce the amount of computational effort, we have made use of lookup tables. The electric field and potential on a grid of positions were precalculated, using a numerical method of solving Poisson's equation (Hoyles et al., 1996), and then recorded in a set of tables. By interpolating between table entries, the electric field and potential anywhere in and in the vicinity of the channel can be quickly determined. Technical details of this method will be described elsewhere (Hoyles et al., 1998).

The electric potential  $V$  experienced by an ion is composed of the following four parts:

$$V_i = V_{S,i} + V_{X,i} + \sum_{j \neq i} V_{I,ij} + \sum_{j \neq i} V_{C,ij}, \quad (5)$$

where the index  $i$  labels ions and the four terms on the right-hand side of the equation are 1) the self-potential due to charges induced by ion  $i$ ; 2) the external potential due to the applied field, fixed charges in the protein wall, and charges induced by these; 3) the image potential due to charges induced by ion  $j$ ; and 4) the Coulomb potential due to the charge on ion  $j$ . We decompose the electric field  $\mathcal{E}$  experienced by an ion in the same way:

$$\mathcal{E}_i = \mathcal{E}_{S,i} + \mathcal{E}_{X,i} + \sum_{j \neq i} \mathcal{E}_{I,ij} + \sum_{j \neq i} \mathcal{E}_{C,ij}. \quad (6)$$

the first three components in Eqs. 5 and 6 were stored in the tables, whereas the Coulomb potential between each pair of ions was computed directly.

To allow rapid lookup, the precalculated results must be on an evenly spaced grid. Because the use of a rectilinear grid would result in many wasted points and a jagged edge near the pore boundary, we made use of a system of generalized cylindrical coordinates for constructing the lookup tables. The position of an ion was first converted to generalized coordinates, and then the values of the electric potential and field in the vicinity of the ion were extracted from the tables by multidimensional linear interpolation, which is a simple algorithm that generalizes easily to dimensions greater than 2 (Press et al., 1989). We used separate tables for the self-potential ( $V_{S,i}$ ), the external potential ( $V_{X,i}$ ), and the image potential ( $V_{I,ij}$ ). These are, respectively, two-, three-, and five-dimensional tables. Cylindrical symmetry has been exploited to reduce by one the number of dimensions of the self-potential and image-potential tables. The electric field was stored and extracted in the same way as the potential, except that three values were required for each point in a table, one for each Cartesian component of the field. So while the field tables were indexed by generalized coordinates, their contents were stored as Cartesian coordinates.

Illustrated in Fig. 2 are a graph of potential energy ( $A$ ) and that of the  $z$  component of force ( $B$ ) for a single ion moving parallel to the central axis of a catenary channel with no dipoles. The solid lines are calculated by using an iterative method (Hoyles et al., 1996), and the circles by interpolating from the precalculated values stored in the lookup tables. The spacing between points in the lookup table is  $1.77 \text{ Å}$  in the  $z$  direction, and the circles are at the midpoints of these intervals, where the maximum interpolation error is expected to occur. There are  $37$  points across the lookup table in the  $r$  direction (perpendicular to the  $z$  axis), and the spacing between these varies with the radius of the channel. As indicated in the inset of Fig. 2, the path of the ion is offset from the  $z$  axis by  $3 \text{ Å}$ , and the ion passes through the midpoint of the radial interpolation intervals in the neck region.

The correspondence between the iterative and lookup methods evident in Fig. 2 indicates that interpolation error is negligible for potential energy and the  $z$  component of force

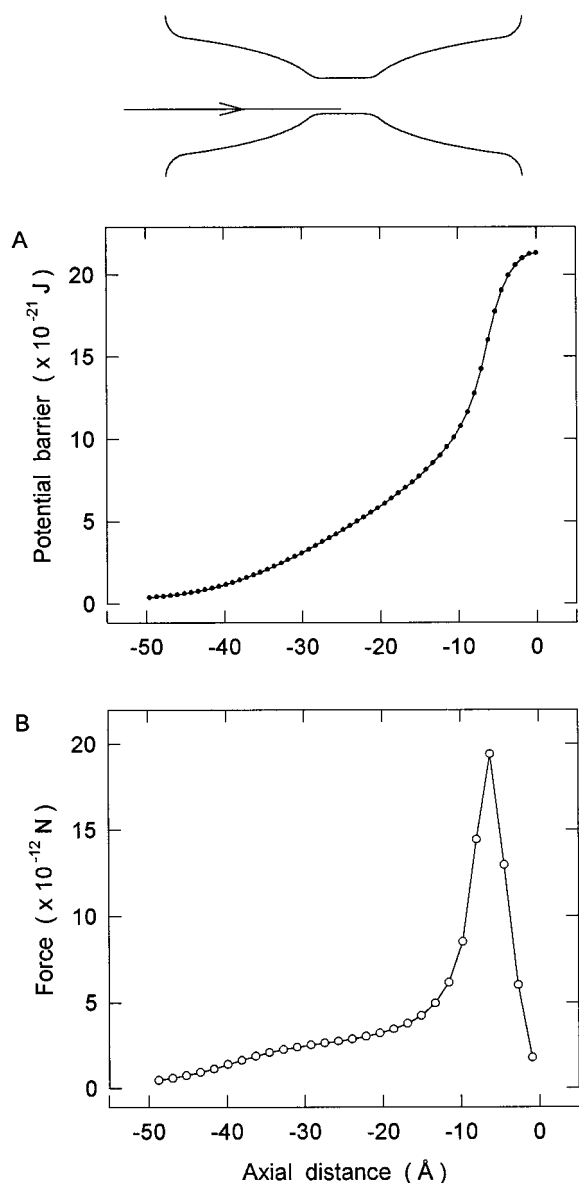


FIGURE 2 A potential energy profile (A) and the  $z$  component of force (B) obtained by interpolating from the precalculated values stored in the lookup tables. An ion was moved along a trajectory that is parallel to the central axis but is offset from it by 3 Å, as indicated by the arrow in the inset. The position of each circle is located at the midpoint between two adjacent points stored in the lookup table. The solid lines passing through the filled circles (potential energy) and open circles ( $z$  component of force) are calculated by using an iterative numerical method.

in the most important parts of the channel, namely, the center of the vestibule and the neck region. More detailed tests indicate that the relative error increases when an ion approaches the vestibular wall. For example, at 1 Å from the wall, the relative error in the repulsive force is  $\sim 15\%$ . This is not of great concern, because ions in the vestibule tend to stay away from the water-protein boundary (Li et al., 1998). In the constricted region, where ions are forced into closer proximity with the wall, the error in the repulsive force 1 Å from the wall is  $\sim 5\%$ .

### Input parameters and details of simulations

Simulations under various conditions, each lasting between 500,000 and 2,000,000 time steps, were repeated many times, for five to nine trials. For the first trial, the positions of ions in the reservoirs were assigned randomly with the proviso that the minimum ion-ion distance should be 2.7 Å, or 1.5 times the radius of a chloride ion. We note that with all subsequent ion-ion distance checking, to be explained below, the minimum allowed distance, which we refer to as the "safe distance," was chosen to be 3/4 of the sum of the ionic radii. For successive trials, the positions of the ions in the last time step were used as the initial starting positions of the following trial. The current (in pA) was extrapolated from the total number of ions traversing the channel over the simulation period.

On each side of the vestibule, a cylindrical reservoir with radius 30 Å and an adjustable height was placed. A fixed number of sodium and chloride ions were placed in each reservoir, and the height of the cylindrical reservoir was adjusted to give a desired ionic concentration. As ions were forbidden to approach the wall of the reservoir within 1 Å, the effective radius of the cylindrical reservoir was 29 Å. For example, if 13 sodium and 13 chloride ions were placed in each reservoir and the desired ionic concentration was 300 mM, the height of each of the two cylindrical reservoirs was adjusted to 22 Å.

To prevent two ions from coming too close to each other, a repulsive short-range potential, varying as  $1/r^9$ , was included (Pauling, 1942). This steeply rising potential imitates the repulsive force produced when the electron shells of two ions begin to overlap. When the ionic concentration in the reservoirs was high, ions at times were able to jump large distances and end up very close to another ion. The forces at the next time step in such instances would be very large, and the affected ions could leave the system. To correct this problem, we checked ion-ion distances at each time step. If two ions were closer than the defined safe distance, then their trajectories were traced backward in time until such a distance was exceeded. By performing these checks and corrections, the system was well behaved over the simulation, even for very high concentration. Such a minor readjustment of the position of an ion was needed about once every 100 time steps when the reservoirs and the channel contained 52 ions. The steep repulsive force at the dielectric boundary due to the image charges was usually sufficient to prevent ions from entering the channel protein. We ensured that no ions would appear inside the channel protein by erecting an impermeable glass boundary at the water-protein interface. Any ion colliding with this boundary was elastically scattered. A similar glass boundary was implemented for the reservoir boundaries.

To ensure that the desired intracellular and extracellular ion concentrations were maintained throughout the simulation, a stochastic boundary was applied. When an ion crossed the transmembrane segment, an ion of the same species was transplanted so as to maintain the original

concentrations on both sides of the membrane. For example, if a sodium ion from the left-hand side of the channel crossed the narrow transmembrane segment and reached the imaginary plane at  $z = 10 \text{ \AA}$ , then the furthest sodium ion in the right-hand reservoir was taken out and placed in the far left-hand side of the left reservoir. When transplanting ions, we chose a point no closer to another ion than the defined safe distance. The stochastic boundary trigger points, located at  $z = \pm 10 \text{ \AA}$ , were checked at each time step of the simulation.

The Brownian dynamics program was written in FORTRAN, vectorized, and executed on a supercomputer (Fujitsu VPP-300). The amount of vectorization varied from 67% to 92%, depending on the number of ions in the reservoirs. With 52 ions in the reservoirs, the CPU time of a supercomputer needed to complete a simulation period of  $1.0 \text{ \mu s}$  (10 million time steps) was  $\sim 18.7 \text{ h}$ . The following physical constants were employed in our calculations:

Dielectric constants:  $\epsilon_{\text{water}} = 80$ ,  $\epsilon_{\text{prot}} = 2$   
 Masses:  $m_{\text{Na}} = 3.8 \times 10^{-26} \text{ kg}$ ,  $m_{\text{Cl}} = 5.9 \times 10^{-26} \text{ kg}$   
 Diffusion coefficients:  $D_{\text{Na}} = 1.33 \times 10^{-9} \text{ m}^2 \text{ s}^{-1}$ ,  
 $D_{\text{Cl}} = 2.03 \times 10^{-9} \text{ m}^2 \text{ s}^{-1}$   
 Relaxation time constants,  $\gamma^{-1}$ :  $\gamma_{\text{Na}} = 8.1 \times 10^{13} \text{ s}^{-1}$ ,  
 $\gamma_{\text{Cl}} = 3.4 \times 10^{13} \text{ s}^{-1}$   
 Ion radii:  $r_{\text{Na}} = 0.95 \text{ \AA}$ ,  $r_{\text{Cl}} = 1.81 \text{ \AA}$   
 Room temperature:  $T_r = 298 \text{ K}$   
 Boltzmann constant:  $k = 1.38 \times 10^{-23} \text{ J K}^{-1}$   
 Elementary charge:  $e = 1.60 \times 10^{-19} \text{ C}$

Throughout we give energy in temperature units,  $kT_r$ . We note that  $1 kT_r$  equals  $4.11 \times 10^{-21} \text{ J}$  and  $2.478 \text{ kJ/mol}$ . Units of dipole moments are quoted in Coulomb-meters, abbreviated hereafter as Cm. One Debye corresponds to  $\sim 3.33 \times 10^{-30} \text{ Cm}$ .

## RESULTS

### Dipoles in the channel

In the absence of any charge moieties or dipoles on the protein wall, the potential barrier presented to an ion moving under the influence of an applied potential of 100 mV is shown in Fig. 3 (*top curve*, labeled 0). The potential energy of a sodium ion placed at a fixed position on the  $z$  axis was calculated numerically by solving Poisson's equation iteratively, as detailed previously (Hoyle et al., 1996). The ion was then moved by  $1 \text{ \AA}$  and the calculations were repeated. The potential profile presented to the ion as it moved from outside (left-hand side) to inside (right-hand side) increased slowly, peaking at the center of the cylindrical transmembrane segment (labeled  $0 \text{ \AA}$ ), and then decreased steadily as it traversed the second half of the channel. Note that without the membrane potential, one would have obtained a symmetrical, bell-shaped barrier with a peak height of  $14.5 \times 10^{-21} \text{ J}$ . The presence of the membrane potential had lowered the relative height of the barrier to  $3.5 \times 10^{-21} \text{ J}$  and distorted the shape of the profile to an asymmetrical curve.

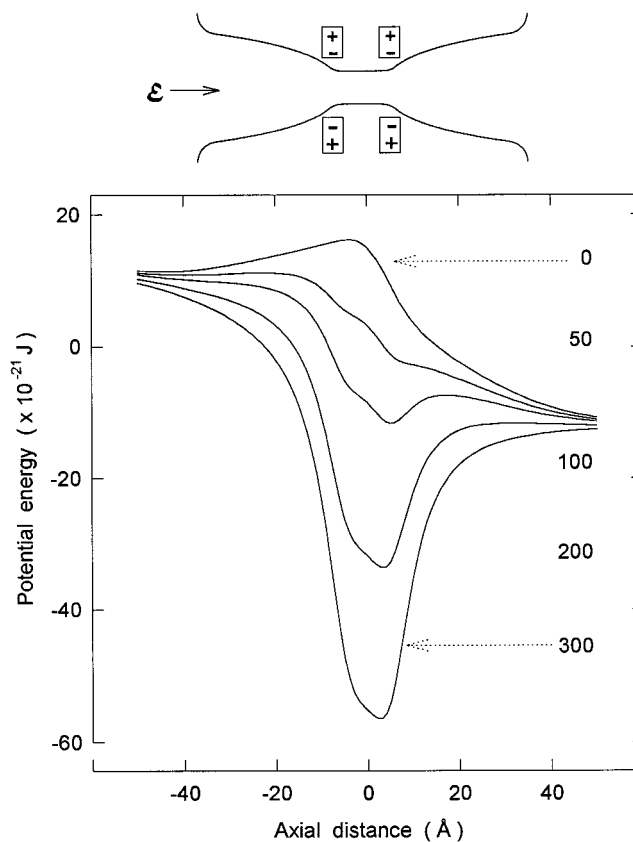


FIGURE 3 Changes in the potential profile with dipole strength. The potential barrier presented to a cation is plotted against its position along its trajectory. A membrane potential of 100 mV was applied such that inside (*right-hand side*) was negative with respect to outside (*left-hand side*). The value at each position was computed from a numerical method of solving Poisson's equation. The uppermost curve, labeled 0, was obtained in the absence of dipoles on the channel wall. The next four curves represent the potential profiles encountered by a cation traversing the channel in the presence of dipoles with strengths of, respectively, 50, 100, 200 and  $300 \times 10^{-30} \text{ Cm}$ . The approximate positions of four of the eight dipoles in the channel are indicated in the inset. The remaining four dipoles are on the plane orthogonal to those shown.

Two rings of dipoles, together with an applied electric potential of 100 mV, eliminated the repulsive dielectric force. The number accompanying each curve in Fig. 3 represents the total strength of four dipoles ( $\times 10^{-30} \text{ Cm}$ ) in each ring. Because there were two rings of dipoles, one at  $z = -5 \text{ \AA}$  and the other at  $z = +5 \text{ \AA}$ , the strength of dipoles placed on the entire channel wall was twice the value indicated in the figure. In the presence of dipoles, an ion traversing from outside to inside would encounter an attractive potential throughout its trajectory. With each stepwise increase in dipole strength, what used to be a potential barrier became a potential well whose depth increased with the strength of dipole moments.

The potential profiles illustrated in Fig. 3 were constructed under the assumption that there were no other ions in the system. Such profiles merely reveal that the permeation of ions across the channel would be hindered if no dipoles were present on the channel wall. It is not possible,

however, to deduce the conductance of the channel from such profiles, or the effect a deep potential well will have on ions permeating the channel. To study these properties, one needs a dynamical theory.

We have used Brownian dynamics simulations to deduce the conductance of the model channel under various conditions. In all of the subsequent figures, unless stated otherwise, each point is the average of nine simulations, each lasting for 500,000 time steps (50 ns), or five simulations, each lasting for 2,000,000 time steps (200 ns). The error bar accompanying each data point is one standard error of mean. The error bar is not shown if it is smaller than the size of the data point. Again, unless noted otherwise, 13 sodium and 13 chloride ions were placed in the left-hand reservoir (representing the extracellular space), whose volume was  $5.84 \times 10^{-26} \text{ m}^3$ , and the same number of ions in the right-hand side reservoir (the intracellular space). Thus the ionic concentration in the reservoirs was 300 mM, which is about double the physiological concentration. This higher concentration was preferred in the simulations to obtain better statistics.

In Fig. 4, the number of ions that traversed the channel under the driving force of 100 mV during a simulation period of  $0.45 \mu\text{s}$  (4.5 million time steps) is converted to current in pA and plotted against the dipole strength. On the right-hand ordinate of Fig. 4, current in pA is converted to conductance in pS at the physiological concentration of 150 mM. Because the current in these ranges of ionic concentrations increases almost linearly with concentration (see later), such an extrapolation of conductance results is justified. With no dipoles placed on the channel wall, the number of sodium ions that traversed from outside to inside in  $0.45 \mu\text{s}$  was 10, which corresponds to a current of 3.6 pA. The net current increased rapidly with the increasing dipole strength up to  $100 \times 10^{-30} \text{ Cm}$  (filled circles in Fig. 4). The number of ions crossing the channel increased further with a further increase in the dipole strength, but many ions were also traversing in the opposite direction, against the direction of the applied electric field. The current flowing from inside to outside is indicated as open circles in Fig. 4. As a result, the net current actually decreased as the dipole strength was increased further from 300 to  $600 \times 10^{-30} \text{ Cm}$ .

The strength of dipoles in biological ion channels is likely to be sufficiently large to cancel the repulsive dielectric force presented to the ion, but not so strong as to allow ions to move against the applied electric gradient. If we assume that the channel shape can be idealized as our model channel and that the dielectric constant of water in the vestibule is 80, then the optimal strength of dipoles on the channel wall is between 100 and  $200 \times 10^{-30} \text{ Cm}$ . In reality, the total dipole moment present on the channel wall will be greater than the value we quote, because the dielectric constant of water in the vestibule must almost certainly be lower than that in bulk water (see, for example, Gutman et al., 1992; Sansom et al. 1997). Hereafter, we place two rings of dipoles, each with a moment of  $100 \times 10^{-30} \text{ Cm}$ , just

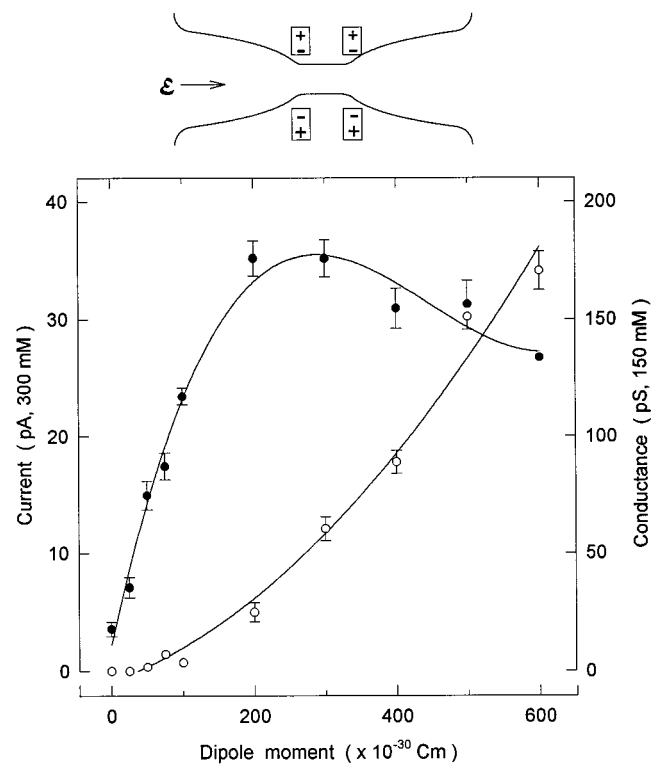


FIGURE 4 Channel conductance as a function of dipole strength. The magnitudes of sodium currents flowing across the channel in the presence of a membrane potential of 100 mV are plotted against strengths of dipoles. The ionic concentration of the reservoir was 300 mM. The left-hand side of the ordinate indicates the current in pA at 300 mM, whereas the right-hand side of the ordinate indicates the conductance in pS at 150 mM. The filled circles show the net current, i.e., the sum of currents in both directions, which flows from outside to inside. The open circles show the current flowing against the potential gradient, namely, from inside to outside. The simulation time for each data point was  $0.45 \mu\text{s}$ , except the value for  $100 \times 10^{-30} \text{ Cm}$ , which was  $2 \mu\text{s}$ . The points were fitted with a polynomial function.

above and below the transmembrane segment to investigate other macroscopically observable properties of membrane ion channels.

### Energy barrier near the transmembrane segment

It is not known how large an energy barrier an ion must overcome to cross the transmembrane segment of the channel. From the conductance-temperature relationship, it has been estimated that the height of this barrier is  $\sim 3 kT_r$  (Kuyucak and Chung, 1994). Here we examine how the height of such a barrier influences the conductance of the channel.

The number of ions crossing the channel was tabulated at a given height of this step potential barrier during the simulation period of  $1.0 \mu\text{s}$ . The current was not attenuated appreciably when the height of the barrier was less than  $1.0 kT_r$ . The channel currents obtained in the absence of any barrier and in the presence of a  $1.0 kT_r$  barrier were the same ( $23.7 \pm 1.4$  versus  $22.1 \pm 1.2$  pA). With a further increase



in the barrier height, however, the current was systematically reduced, as shown in Fig. 5. On the right-hand ordinate of Fig. 5, we show the channel conductance at 150 mM concentration. It decreased progressively from 110 pS with an increasing barrier height, dropping to  $52 \pm 7$  pS at  $2.0 kT_r$ . When the barrier height was  $2.5 kT_r$ , this conductance of the channel became approximately the same as that obtained experimentally from the ACh channel (Hamill and Sakmann, 1981) or from the *N*-methyl-D-aspartate-activated channel (Chung and Kuyucak, 1995).

**Ionic concentrations in the channel**

In the volume of our model channel, which is  $2.16 \times 10^{-26}$  m<sup>3</sup>, there would be 720 water molecules. At a concentration of 300 mM, a similar bulk volume would contain four sodium and four chloride ions. Here we examine the number of sodium and chloride ions inside the channel under various conditions. To compute the average number and concentration of sodium and chloride ions inside the channel, we divided the model catenary channel, whose length is 80 Å, into 16 5-Å sections, as shown in the inset of Fig. 6. The volumes of the slices from the outermost layer to the smallest layer in the transmembrane segment were 2.94, 2.18, 1.88, 1.54, 1.16, 0.71, 0.25, and  $0.15 \times 10^{-27}$  m<sup>3</sup>.

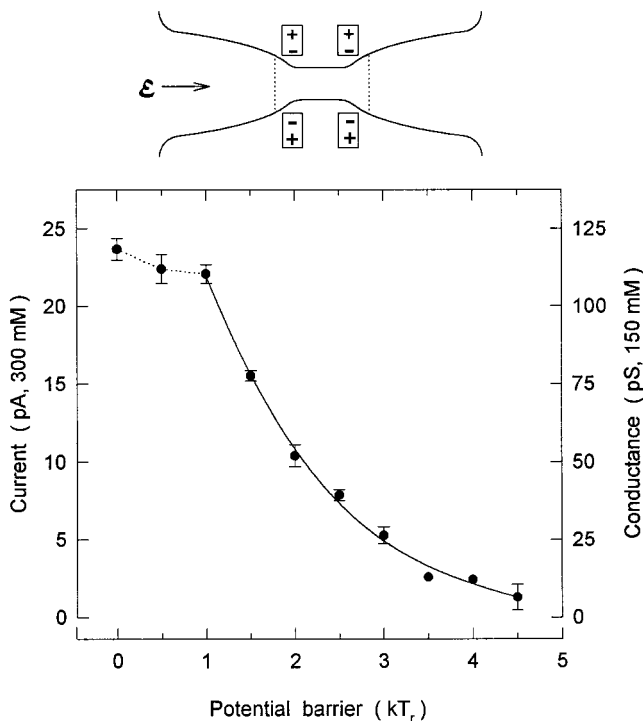


FIGURE 5 Channel conductance as a function of the height of the potential barrier. The total strength of dipoles in each ring was  $100 \times 10^{-30}$  Cm, and a membrane potential of 100 mV was applied throughout. A step potential barrier was placed within  $z = \pm 10$  Å, as indicated in the inset. The current across the channel at 300 mM (left-hand ordinate) and the channel conductance at 150 mM (right-hand ordinate) decreased steadily as the barrier height increased. Each point was obtained from a total simulation period of 1.0 μs.

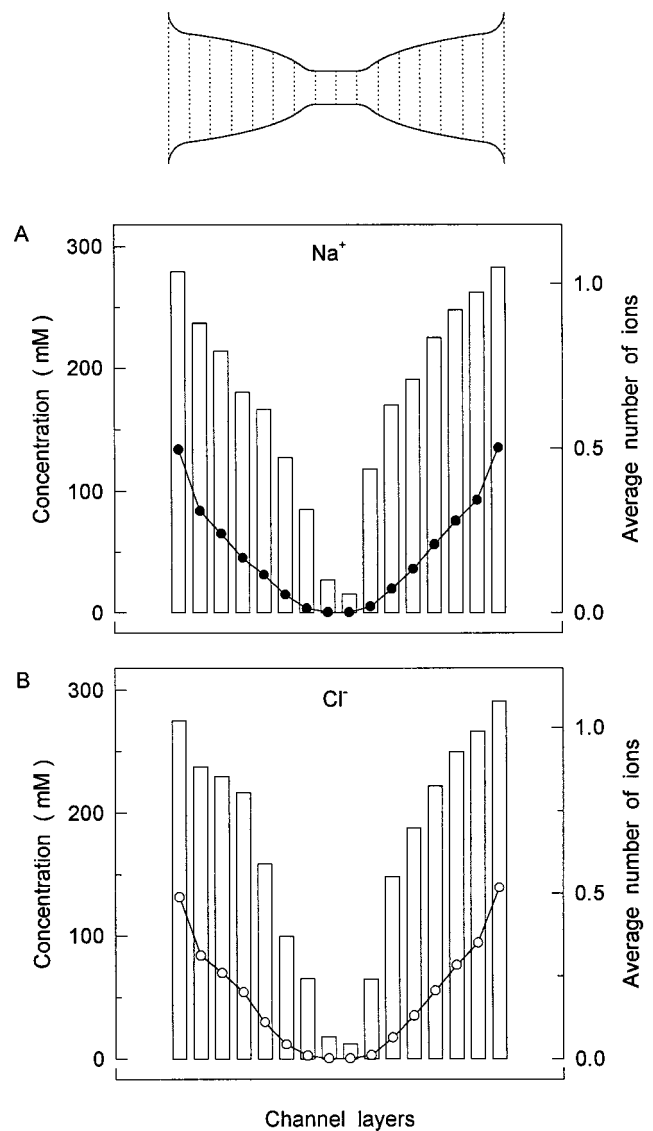


FIGURE 6 Concentrations of sodium and chloride ions in the channel. The model channel was divided into 16 5-Å-thick sections, as indicated in the inset, and the average number of ions present over the simulation period of 0.45 μs in each section was tabulated (filled and open circles). The ionic concentration in each section was then calculated by dividing the average number of ions in each section by its volume (bars). The concentration of sodium (and chloride) ions in the reservoirs was 300 mM in this and the following three figures. With no dipoles on the channel wall and no applied electric field, the probability of sodium ions (A) and chloride ions (B) being in each section decreased steadily with its distance from the reservoir.

In the absence of a membrane potential and dipoles in the protein, ions were virtually excluded from entering the vestibule neck, owing to the repulsive dielectric force presented to them by the dielectric wall. In Fig. 6, A and B, the time averages of sodium and chloride concentrations in the channel are illustrated. The number of ions present in each layer per unit time was first tabulated (filled and open circles), and then the concentration in each layer was derived by taking into account its volume. The average ionic concentration in each of the two outermost layers was

$\sim 10\%$  lower than that in the adjoining reservoir, which was 300 mM. The ionic concentration in successive layers declined progressively, dropping to less than 10% of the reservoir value in the neck region.

When a membrane potential of 100 mV was applied across the channel, such that the right-hand reservoir was made negative with respect to the left-hand side, there was a small but consistent increase in the concentration of sodium ions in the left vestibule and in the concentration of chloride ions in the right vestibule (Fig. 7). Other than this small asymmetry in the concentrations and a slight increase in the probability of ions being present in the constricted segment, the applied field had little effect on the average

concentrations in the channel. A drastic change in the pattern of charge densities occurred when, instead of applying an electric potential across the channel, two rings of dipoles were placed on the channel wall. As shown in Fig. 8, there was a marked increase in the concentration of sodium ions in the constricted region of the channel. Sodium ions entering the channel occasionally would become detained in the potential well created by the dipoles on the wall. Some ions jumped from one well to the other and drifted across the other side, but because there was no potential gradient, the number of ions drifting in one direction ( $11.7 \pm 1.3$  pA) was about the same as that in the opposite direction ( $10.7 \pm 1.3$  pA).

To mimic the concentration gradient in the channel during its open state, we placed an energy barrier of  $1.5 kT_r$  at

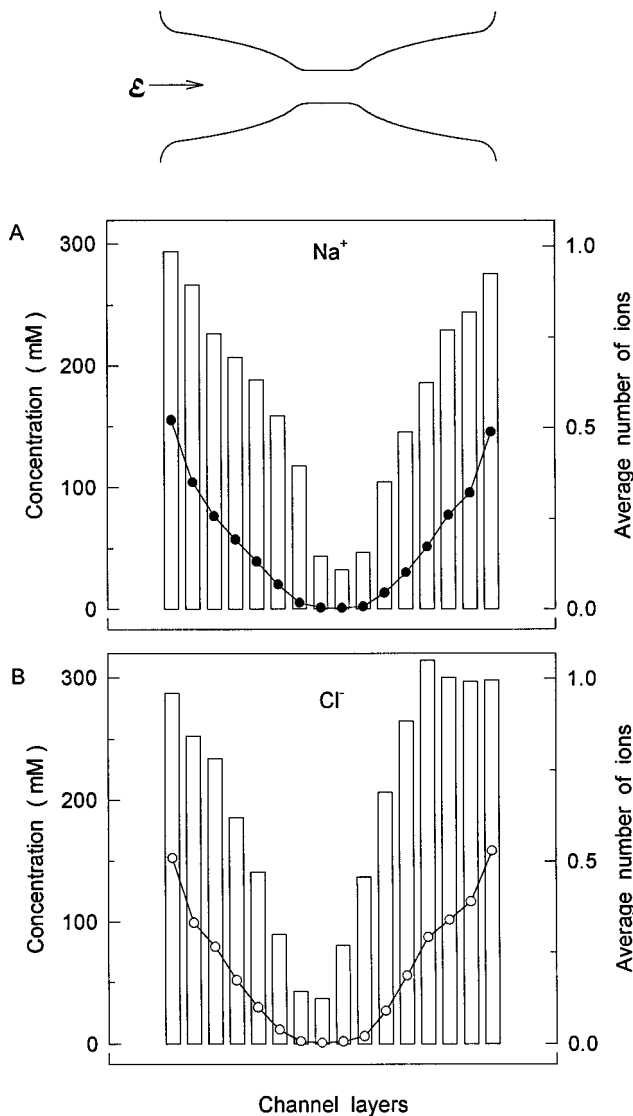


FIGURE 7 Concentrations of sodium and chloride ions in the channel in the presence of a membrane potential  $\mathcal{E}$ . When a membrane potential of 100 mV was applied, as shown in the inset, there was a small increase in the concentration of sodium ions in the left-hand vestibule (A), and a similar but slightly larger increase in chloride ions in the right-hand vestibule (B). The difference is due to the larger diffusion coefficient of chloride ions compared to that of sodium ions.

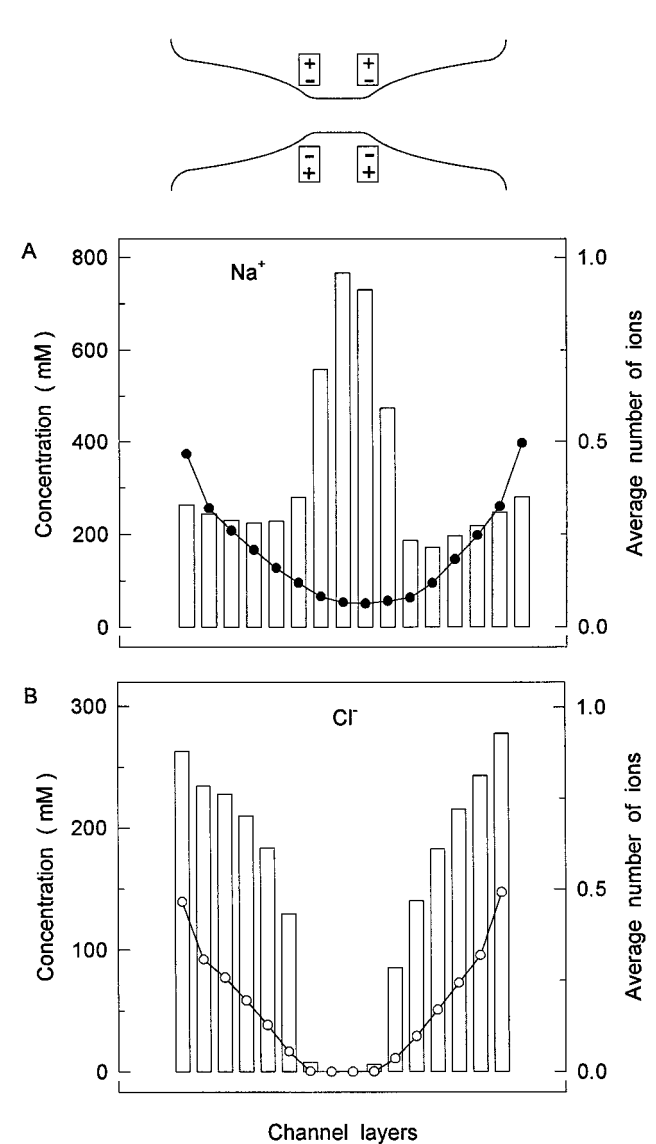


FIGURE 8 Concentrations of sodium and chloride ions in the channel in the presence of two dipole rings. Each dipole ring, with a total moment of  $100 \times 10^{-30}$  Cm, was placed in the positions indicated in the inset. There was a large increase in the concentrations of sodium ions in the innermost sections of the channel (A). In contrast, chloride ions were excluded from the innermost sections (B).

the constricted segment and applied a membrane potential of 100 mV. As shown in Fig. 9, the sodium concentration in all layers of the channel was approximately constant under these conditions and ions moved steadily from outside to inside, without being detained by the dipoles on the channel wall. In contrast, chloride ions were virtually excluded from entering the inside of the channel (Fig. 9 B). The conductance of the channel under this condition was  $78 \pm 4$  pS at 150 mM (or  $15.5 \pm 0.7$  pA at 300 mM), and no sodium ions traversed against the potential gradient.

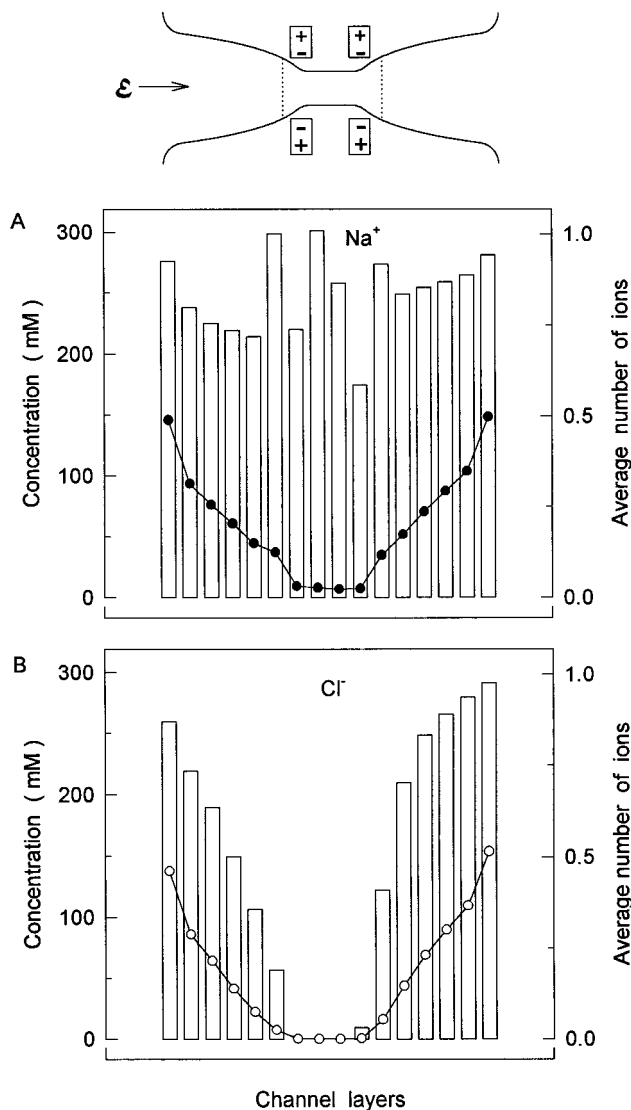


FIGURE 9 Concentrations of sodium and chloride ions in the presence of dipoles and an applied electric field. Two potential barriers of  $1.5 kT_r$  were placed at the positions indicated in the inset. With two rings of dipoles canceling the repulsive dielectric force and a driving force provided by a membrane potential of 100 mV, sodium ions steadily traversed the channel. The concentrations of sodium ions in all sections of the channel remained approximately constant (A). In contrast, chloride ions were virtually excluded from the transmembrane sections (B).

### Current-voltage relationships

The current-voltage relationships obtained from excised single channels are in general ohmic, although some show some pronounced inward or outward rectification. The reversal potential observed in asymmetrical ionic solutions closely matches that predicted by the Nernst equation. Here we show how the presence of an energy barrier in the channel can distort the linear current-voltage relation.

The current increased linearly with the applied voltage, as shown in Fig. 10 A, when there was no additional potential

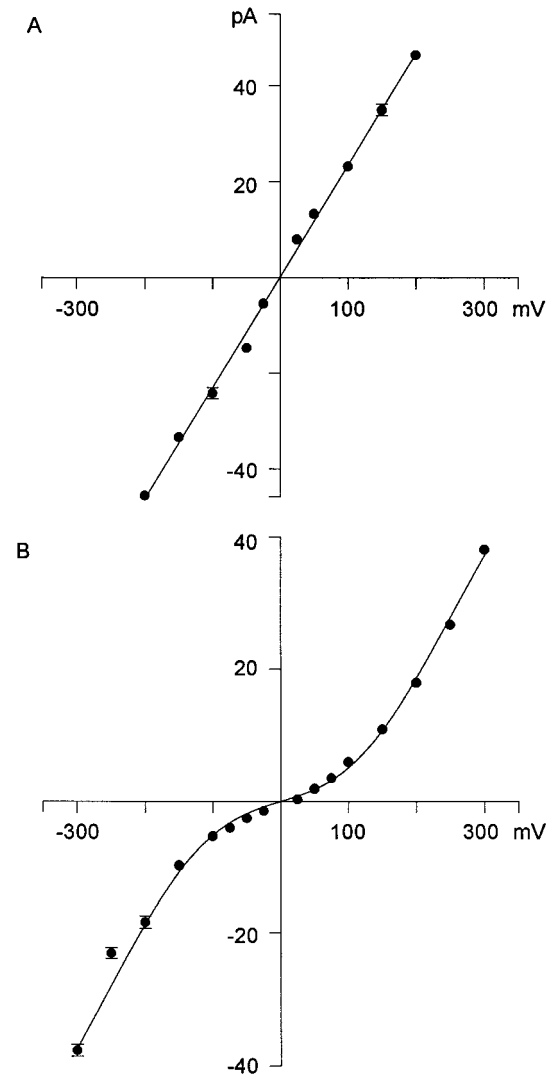


FIGURE 10 Current-voltage relationships obtained with symmetrical solutions. (A) The currents flowing across the channel that had no potential barrier near the entrance of the transmembrane segment were measured at different applied potentials. Two rings of dipoles, each ring with the strength of  $100 \times 10^{30}$  Cm, were placed on the channel wall. The current-voltage relationship obtained under these conditions is ohmic. The slope of the line drawn through the data points is  $232 \pm 4$  pS. (B) When a potential barrier of  $3.0 kT_r$  was erected, the current-voltage relationships became nonlinear. The data points were fitted with a modified Ohm's law that takes the barrier into account (see Eq. 12). The values of  $\gamma$  and  $\beta$  used to fit the curve were, respectively,  $142 \pm 4$  and  $3.5 \pm 0.4$ . The simulation period used to obtain each data point was 1  $\mu$ s.

barrier in the channel presented to ions for penetrating the transmembrane segment. In this and all subsequent current-voltage curves, we used the total strength of four dipoles in each ring of  $100 \times 10^{-30}$  Cm. The core conductance of the channel, deduced from the regression line of the form,  $I = \gamma V$ , fitted through the data points, was  $232 \pm 4$  pS (or 116 pS at 150 mM). When an energy barrier of  $3.0 kT_r$  was erected at the entrance of the constricted segment, the current was attenuated, but not by a constant proportion at all voltages. For example, the currents in the absence and presence of this barrier at 200 mV were, respectively, 46.0 pA and 18.2 pA (39.6%). With the applied potential of 50 mV, however, the current was reduced from 14.0 pA to 2.2 pA (15.7%), thus indicating that the barrier of the same height became less of an impediment when the driving force was large. With a  $3.0 kT_r$  barrier, the current-voltage relationship became nonlinear, deviating markedly from Ohm's law, as shown in Fig. 10 B. The solid line fitted through the data points in Fig. 10 B was calculated from the Pöschl-Teller function of the form  $I = \gamma V/[1 + \beta \operatorname{sech} x]$ , where  $x = eV/V_B$  and  $V_B$  is the barrier height. The justification for fitting the data with this function is given in the Discussion section. The values of  $\gamma$  and  $\beta$  used to generate the curves shown in solid lines are given in the figure legend.

Fig. 11 A shows the current-voltage relationship obtained with asymmetrical ionic solutions in the two reservoirs. The ionic concentrations outside (left-hand reservoir) and inside (right-hand reservoir) were 480 mM and 120 mM, respectively. To make the solution electrically neutral, the same number of sodium and chloride ions was placed in each reservoir. With no energy barrier in the channel, the slope for the outward current (at the positive potential, *filled circles*) was steeper than that predicted by the Goldman equation. Then we added potassium ions such that the number of cations (sodium and potassium) in one reservoir was equal to that in the other reservoir. Thus the ionic concentrations outside were 480 mM NaCl and 120 mM KCl, whereas those inside were 120 mM NaCl and 480 mM KCl. Potassium ions were prevented from entering the constricted region of the channel by erecting two impermeable barriers at  $z = \pm 10 \text{ \AA}$ . Potassium ions colliding with these barriers were elastically scattered. The slope of the outward current (*open circles*) obtained under these conditions was less steep than that predicted by the Goldman equation. The solid line fitted through the data points was calculated with the Goldman equation of the form

$$I = KV \frac{1 - 4 \exp(-eV/kT)}{1 - \exp(-eV/kT)}, \quad (7)$$

where  $K$  is a constant and the factor of 4 arises from the outside to inside ratio of concentrations.

The slope of the outward current was affected more markedly by the presence of impermeable potassium ions when the concentration ratio was 2:1, as illustrated in Fig. 11 B. In these simulations, the ionic concentrations of NaCl outside and inside were, respectively, 400 mM and 200 mM.

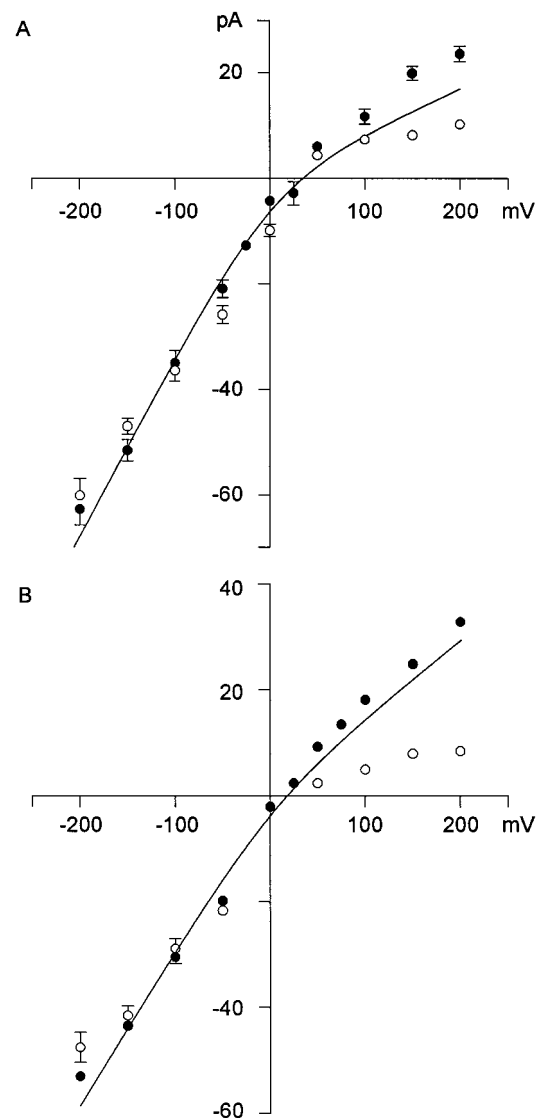


FIGURE 11 Current-voltage relationships obtained with asymmetrical solutions. The strength of dipoles placed on the channel wall was the same as in Fig. 10. Each point in this figure represents the average of five simulations, each simulation lasting for 2,000,000 time steps (200 ns). (A) The current-voltage relationship was first obtained with the ionic concentrations of 480 mM outside and 120 mM inside (●). Then, the ionic strengths were changed such that the outside contained 120 mM KCl (and 480 mM NaCl) and the inside contained 480 mM KCl (and 120 mM NaCl), and the channel was made impermeable to potassium ions. The outward current was markedly depressed in the presence of potassium ions (○). (B) The current-voltage relationship was obtained with ionic solutions of 400 mM outside and 200 mM inside (●). Then 200 mM KCl was added to the outside solution and 400 mM KCl to the inside solution. The outward current was depressed in the presence of potassium ions (○). The solid lines drawn through the data point were calculated with a Goldman equation of the form given in Eq. 7, with the constant  $K = 0.085$  for A and  $K = 0.146$  for B.

With no potassium ions, the magnitude of the inward current at a given applied potential is about half that of the outward current (*filled circles*). The currents flowing across the channel at various holding potentials were determined again with 200 mM KCl added to the extracellular solution

and 400 mM KCl to the intracellular solution. Thus the total cation concentrations inside and outside in these simulations were 600 mM. As shown in Fig. 11 B, the outward current was appreciably attenuated, whereas the inward current remained unchanged (*open circles*). The solid line was again calculated from the Goldman equation, with the pre-exponential factor of 2 in the numerator of Eq. 7.

From a series of simulations such as those illustrated in Fig. 11, we conclude that the Nernst equation correctly predicts the reversal potential when the ionic concentrations in the two faces of the channel are different. The relative steepness of the slopes fitted through inward and outward currents changes appreciably when other cations that are impermeable to the channel are present. The shape of the current-voltage relationship is further distorted when an energy barrier is erected near the constricted segment of the channel.

### Conductance-concentration curve

Experimentally, current across a biological ion channel increases monotonically with an increasing ionic concentration initially and then saturates with a further increase in concentration (Hille, 1992). Saturation of channel currents occurs when there is a rate-limiting permeation process that is independent of ionic concentrations. For example, an ion arriving near the constricted membrane segment will be detained there for a period of time if, before traversing the narrow pore, it needs to gain a sufficient kinetic energy to climb over an energy barrier. The reason for the presence of such a barrier is explained in the Methods.

In Fig. 12, the conductance of the channel is plotted against the concentrations of sodium ions in the reservoirs. The two reservoirs contained an equal number of sodium-chloride pairs, and an applied membrane potential of  $-100$  mV provided the driving force for sodium ions to move inward. The presence of two rings of dipoles, with their negative poles pointing to the lumen, ensured that the channel was selectively permeable to sodium ions. When the channel had no potential barrier, the ionic current carried by sodium ions increased linearly with concentration, as shown in Fig. 12 A. Because the magnitude of the current in this series of simulations was large, we used the total simulation period of  $0.225 \mu\text{s}$  for each point shown in Fig. 12 A. The linear conductance-concentration relation became distorted when a barrier was placed  $5 \text{ \AA}$  from each end of the cylindrical pore. Fig. 12 B illustrates the conductance-concentration curve obtained from the channel with a step potential barrier of  $3.0 kT_r$ . The ordinate of Fig. 12 B is expanded, because the currents were greatly attenuated by the presence of the barrier. At a low ionic concentration, the conductance was nearly proportional to the ionic concentration. As the ionic concentration was increased, however, the conductance increased less with increasing concentrations. We fitted the points with the curve calculated from the

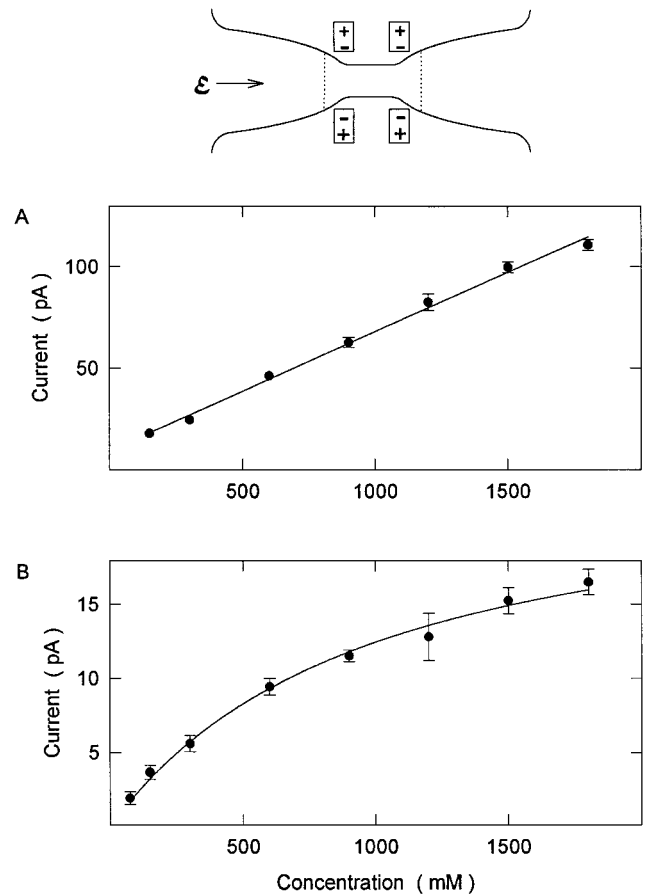


FIGURE 12 Conductance-concentration curve. The ionic concentrations in the two reservoirs were systematically increased while keeping the strength of dipoles and an applied membrane potential constant at  $100 \times 10^{-30}$  Cm and 100 mV, respectively. The number of ion pairs in each reservoir, with the radius of 30 Å, ranged from 3 (for 75 mM) to 78 (for 1800 mM). (A) With no barrier present, the current increased linearly with ionic concentrations. Each point represents the average of nine trials, with each trial lasting for 250,000 time steps or  $0.225 \mu\text{s}$ . (B) When a step barrier with a height of  $3.0 kT_r$  was erected  $5 \text{ \AA}$  from the entrance of the transmembrane segment, the conductance-concentration relation became nonlinear. The current increased linearly with an increasing ionic concentration at first and then began to saturate. The data points of B were fitted to Eq. 8. The simulation period for each point in B was  $1 \mu\text{s}$ , except for those representing 1.2, 1.5, and 1.8 M, for which simulation periods of  $0.3 \mu\text{s}$  were used.

Michaelis-Menten equation of the form

$$I = \frac{I_{\max}}{1 + K_s/[c]} \quad (8)$$

where  $I_{\max}$  and  $K_s$  are the fit parameters. For the solid line drawn through the data points of Fig. 12 B, the numerical values of these two parameters are  $I_{\max} = 25 \pm 5$  pA and  $K_s = 996 \pm 351$  mM. In the Discussion we give a plausible physical interpretation of Eq. 8.

### DISCUSSION

As we have demonstrated here and elsewhere (Li et al., 1998), the Brownian dynamics algorithm devised by van

Gunsteren and Berendsen (1982) is highly suitable for studying the motions of interacting ions in a fluid. One of the major advantages of this algorithm is that the range of time steps  $\Delta t$  is not restricted by the relaxation time constant ( $\gamma^{-1}$ ) as  $\Delta t \ll \gamma^{-1}$ , which is the case in most other Brownian dynamics algorithms. At room temperature, the relaxation time constant for sodium ions is on the order of 10 fs; thus, to meet the condition stipulated in this equation, a time step on the order of 1 fs must be used with such algorithms. As the computational cost of covering a simulation period of a few microseconds would be prohibitively expensive, the use of such algorithms in studying the permeation of ions across biological channels is severely limited. Our preliminary tests of the van Gunsteren-Berendsen algorithm in a simple periodic boundary and a toroidal dielectric boundary showed that many of the important features of the motions of interacting ions in a fluid could be captured even when a  $\Delta t$  as large as 100 fs is used. Among these important features are mean square displacement, the velocity distribution, and the conductance of bulk electrolyte solutions. Furthermore, the temperature of the system remained stable over the simulation period, and the ionic concentration in a localized region, revealed by the time average of the probability of occupancy, remained constant at 150 mM.

The results of simulations are in agreement with experimental findings in several respects. First, the channel conductance is close to that determined experimentally for the ACh channel when the height of the energy barrier is  $\sim 3.0 kT_r$  or  $1.23 \times 10^{-20}$  J. Second, the current-voltage relationship obtained with symmetrical solutions is close to linear for moderate applied potentials, as is the case with many biological channels. The relationship obtained with asymmetrical solutions shows rectification, with the reversal potential close to that predicted by the Nernst equation. Third, the conductance-concentration curve has the same shape as those observed experimentally, although the saturation concentration is higher than expected. The model also makes a number of other predictions. To render the channel permeable to ions, several charge groups must be placed in the protein wall to counteract the repulsive dielectric force. An excessive number of charge residues, however, allows sodium ions to flow against the potential gradient, so reducing the conductance of the channel. Moreover, counterions do not screen the image repulsion to any great extent, in either the vestibule or the constricted region. Finally, current-voltage curves can be expected to be nonlinear at large potentials, or for channels with large energy barriers.

### Suppression of currents by an energy barrier

A potential barrier presented to an ion, arising from the dehydration and substitution process and the electrostatic interaction between ions and charge multipoles on the wall, will ensure that only the ions with thermal energies  $E$  larger than the barrier height will be allowed to go through the

neck. The probability  $\mathcal{P}$  of an ion surmounting a barrier of height  $V_B$  follows from the Boltzmann distribution as

$$\mathcal{P}(E > V_B) = \frac{2}{\sqrt{\pi}} (kT)^{-3/2} \int_{V_B}^{\infty} \exp[-E/kT] \sqrt{E} dE, \quad (9)$$

the solution of which is given by the incomplete  $\Gamma$  function,

$$\mathcal{P}(E > V_B) = \frac{2}{\sqrt{\pi}} \Gamma\left(\frac{3}{2}, \alpha\right), \quad \alpha = V_B/kT. \quad (10)$$

Using the asymptotic expansion for the incomplete  $\Gamma$  function, Eq. 10 can be written as

$$\begin{aligned} \mathcal{P}(E > V_B) &= \frac{2}{\sqrt{\pi}} \exp(-\alpha) \sqrt{\alpha} \left(1 + \frac{1}{2\alpha} - \frac{1}{4\alpha^2} + \frac{1}{8\alpha^3} - \dots\right). \end{aligned} \quad (11)$$

From Eq. 11, one would predict that the conductance should be attenuated by a factor of 16 when a barrier with a height of  $3 kT_r$  is erected. In contrast, the conductance in our study decreased from 118 pS to 26 pS, or by a factor of 4.5 (see Fig. 5). This is because an ion attempting to surmount a barrier, instead of disappearing after a single try, makes repeated attempts. Coulomb repulsion of another ion approaching the neck region would also enhance the probability of transit, which is an entirely dynamic effect not anticipated in Eq. 9. This illustrates the danger of applying a static equation such as the Boltzmann equation to a dynamic situation.

### Current-voltage relationship

If the ionic concentrations on the two faces of the channel are the same, the current-voltage relationship obtained from patch-clamp recordings is, in general, ohmic. The current-voltage relationship deduced from our simulations becomes nonlinear whenever there is a potential barrier for the ions to surmount to cross the channel (Fig. 10). This deviation from Ohm's law is more pronounced when the potential barrier is large. Although the precise shape of the curve cannot be deduced a priori, it is easy to see how such a curvature in the current-voltage relationship would arise. The presence of a barrier is less of an impediment when the driving force is large. This intuitive observation suggests a modification of Ohm's law with the Pöschl-Teller function

$$I = \frac{\gamma V}{1 + \beta / \cosh(eV/V_B)}, \quad (12)$$

where  $\gamma$  is the conductance,  $V_B$  is the barrier height, and  $\beta$  is a dimensionless constant. When  $eV \gg V_B$ , the denominator goes to 1, and one recovers Ohm's law. For  $eV \ll V_B$ , Eq. 12 is again linear, but with a conductance reduced to  $\gamma V / (1 + \beta)$ . The nonlinearities in the  $I$ - $V$  curves become apparent only when  $eV > V_B$ , which corresponds to the region  $V \approx 100$ – $200$  mV for the above barriers.

That there is a potential barrier in biological ion channels has been inferred from the temperature dependence of channel conductance. The conductance-temperature curve obtained from biological channels is always steeper than the conductivity-temperature curve obtained in bulk electrolyte solutions (see Kuyucak and Chung, 1994; Chung and Kuyucak, 1995; Milburn et al., 1995). A steeper increase in the channel conductance with temperature is expected if we assume that there is an additional barrier presented to ions entering the transmembrane segment. It is possible that current-voltage relations obtained from biological channels may deviate from straight lines, especially at large values of the applied voltage. If such deviations do occur, fitting the data points with Eq. 12 will provide an estimate of the barrier height present in the channel.

When the ionic concentrations in the two sides of the channel differ, it is difficult to predict theoretically how the current will vary as a function of the applied potential, even in the absence of any potential barrier in the channel. On a macroscopic level, the driving force provided to ions with a potential difference and that with a concentration gradient are equivalent, being coupled by the Nernst-Planck equation, and concentration differences are often expressed as an equivalent potential. By making a simplifying assumption that the electric field across the channel is uniform, the Nernst-Planck equation is integrated to obtain an explicit expression for the magnitude of currents flowing across the membrane as a function of the applied potential and the ionic concentrations at the two faces of the membrane. This is the Goldman equation. Although the field across the channel is far from uniform, being grossly distorted by the dielectric boundary (Kuyucak et al., 1998), the measured data points are in reasonable agreement with the predicted values from the Goldman equation (Fig. 11). The relative slopes for the inward and outward currents, however, change in a sensitive way when impermeant ions are placed in the extracellular and intracellular media. When a barrier is introduced in the channel, the shape of the current-voltage relationship becomes further distorted. In a narrow range of the applied voltage, for example, within  $\pm 100$  mV, one could fit the data points with a straight line that intersects the abscissa at the reversal potential predicted by the Nernst equation. If the Goldman equation fails to describe current-voltage relations obtained from real biological channels, the discrepancy, we believe, arises from the presence of a potential barrier in the conduit and impermeant ions, rather than from the constant field assumption that had to be made to integrate the Nernst-Planck equation.

### Ions in the channel

We took ensemble averages of time averages of ionic concentrations in discrete layers of the model channel under various conditions (Figs. 6–9). The main point emerging from these results is that the channel for the most part is devoid of ions. If the outermost layer bordering the reservoir

is excluded, each vestibule on average contains about one sodium ion and one chloride ion when the ionic concentration in the surrounding medium is 300 mM. With no dipoles on the channel wall and no applied electric field, the average number of sodium ions in the channel is the same as the average number of chloride ions in the channel. Thus the time average of the total induced surface charges will be zero, as is the net dielectric force experienced by the ions. One may thus be tempted to conclude that the dielectric force plays no role in electrolyte solutions, because induced surface charges of one polarity are canceled by those of the opposite polarity. In reality, however, single sodium ions and chloride ions stumble into the vestibule at different times; thus each experiences the full repulsive dielectric force arising from induced surface charges. Even if a sodium ion is deliberately placed within 1 Debye length of a chloride ion, its thermal energy is about twice as large as the interaction energy of the ion pair ( $6.0 \times 10^{-21}$  J versus  $2.7 \times 10^{-21}$  J), and one drifts away from the other within a few picoseconds. Therefore, any conclusion derived from theoretical calculations that do not take induced surface charges into account is likely to be flawed.

Ions do not traverse the channel in the absence of dipoles on the channel wall. When an electric potential of 100 mV is applied across the channel, there is a small increase in the average number of sodium ions in one vestibule and a similar increase in chloride ions in the other vestibule (Fig. 7). The driving force provided to ions by the membrane potential is not sufficient to overcome the repulsive dielectric force. Only when dipoles of a favorable orientation are placed on the sides of the transmembrane segment can an ion traverse the channel under the influence of the membrane potential. This raises an intriguing question about whether opening or closing of biological ion channels needs to be steric. Ion channels, in theory, can be gated electrostatically by rotating an appropriate number of charge moieties into and out of the protein lining.

### Current-concentration curve

Experimentally it has been shown that the current first increases with an increasing ionic concentration and then saturates (Rae et al., 1988; Hille, 1992). Such a relationship is expected to be found when the transport of ions across the channel is determined by two independent processes, one of which depends upon ion concentration and one that does not. In our simulations, for example, the time  $\tau_1$  it takes for an ion to arrive near the constricted segment is inversely proportional to the electric field  $\mathcal{E}$  and ionic concentration  $[c]$ , whereas the time  $\tau_2$  it takes for the ion to acquire a sufficient kinetic energy to surmount the barrier placed near the transmembrane segment and traverse the second half of the channel is relatively independent of the ionic concentration but dependent only on the electric field. Thus, assuming a uniform electric field, the transit times can be

written as

$$\tau_1 = \frac{k_1}{[c]\mathcal{E}}, \quad \tau_2 = \frac{k_2}{\mathcal{E}}, \quad (13)$$

where  $k_1$  and  $k_2$  are constants. The total time  $\tau$  it takes an ion to traverse the channel is  $\tau = \tau_1 + \tau_2$ , and the current flowing across it will be  $I = nze$ , where the number  $n$  of ions carrying charges  $ze$  is  $1/\tau$ . Thus the current is inversely proportional to the total transit time, that is,

$$I \propto \frac{ze}{(\tau_1 + \tau_2)} = \frac{ze\mathcal{E}}{k_1/[c] + k_2}. \quad (14)$$

For large concentrations, Eq. 14 approaches a maximum value that we denote by  $I_{\max} = ze\mathcal{E}/k_2$ . Factoring out  $k_2$  and introducing  $K_s = k_1/k_2$ , Eq. 14 can be written in the form

$$I = \frac{I_{\max}}{1 + K_s/[c]}. \quad (15)$$

The form of this equation is identical to that of the Michaelis-Menten equation, which is derived under an entirely different set of assumptions. The curves calculated from Eq. 15 fit the current-concentration relationships obtained from our simulations reasonably well (see Fig. 12).

## CONCLUDING REMARKS

Although the results of our simulations are generally in accord with measurements made from patch-clamp recording techniques, we need to make several refinements in our model channel. First, conclusions drawn and inferences made from electrostatics are not valid in regions that are small compared to the diameter of water and ion molecules. In the constricted region of the channel, where the radius is  $\sim 4 \text{ \AA}$ , water molecules are ordered (see, for example, Sansom et al., 1996) and are not free to align with the external field. To account for the processes of ion permeation inside of this region, we have placed in this study a potential barrier near the entrance of the transmembrane segment. The height of this barrier could be determined from molecular dynamics calculations. Furthermore, in this narrow cylindrical segment, the mobility of ions is drastically reduced, as demonstrated by several molecular dynamics studies (Roux and Karplus, 1991b; Chiu et al., 1993). Thus the values of the friction coefficient in the transmembrane segment need to be different from those in the vestibules. Second, in applying continuum electrostatics to describe long-range interactions between particles, we used the dielectric constant of bulk water. Confined in each channel vestibule are  $\sim 360$  water molecules. Almost certainly the effective dielectric constant (and the diffusion coefficient) of ions in such "vicinal" water will be lower than those in bulk water. Again, they must be first determined from molecular dynamics calculations and then incorporated into the Brownian dynamics algorithm. Third, if the dielectric constant in the vestibule is lower than 80, there

will be an additional energy barrier for an ion entering from the reservoir to the vestibule, resulting from the change in Born energy. After its height is determined, this barrier must also be incorporated into the algorithm. Once these modifications are made, there can be a fruitful interaction between experiment and theory, the former providing hints and clues for further modifications of the model, and the latter making new testable predictions.

This work was supported by grants from the Australian Research Council and the National Health and Medical Research Council of Australia. The calculations upon which this work is based were carried out with the Fujitsu VPP-300 of the ANU Supercomputer Facility.

## REFERENCES

- Bek, S., and E. Jakobsson. 1994. Brownian dynamics study of a multiply-occupied cation channel: application to understanding permeation in potassium channel. *Biophys. J.* 66:1028–1038.
- Chiu, S.-W., and E. Jakobsson. 1989. Stochastic theory of singly occupied ion channels. II. Effects of access resistance and potential gradients extending into the bath. *Biophys. J.* 55:147–157.
- Chiu, S.-W., J. A. Novotny, and E. Jakobsson. 1993. The nature of ion and water barrier crossings in a simulated ion channel. *Biophys. J.* 64: 98–108.
- Chung, S. H., and S. Kuyucak. 1995. Temperature-dependent changes in the characteristics of NMDA-activated channels in hippocampal neurons. *Neurosci. Lett.* 187:181–184.
- Cooper, K., E. Jakobsson, and P. Wolynes. 1985. The theory of ion transport through membrane channels. *Prog. Biophys. Mol. Biol.* 46:51–96.
- Gutman, M., Y. Tsfadia, A. Masad, and E. Nachliel. 1992. Quantitation of physical-chemical properties of the aqueous phase inside the phoE ionic channel. *Biochim. Biophys. Acta.* 1109:141–148.
- Hamill, O. P., and B. Sakmann. 1981. Multiple conductance states of single acetylcholine receptor channels in embryonic muscle cells. *Nature.* 294:462–464.
- Hille, B. 1992. *Ionic Channels of Excitable Membranes*, 2nd Ed., Sinauer Associates, MA.
- Hoyle, M., S. Kuyucak, and S. H. Chung. 1996. Energy barrier presented to ions by the vestibule of the biological membrane channel. *Biophys. J.* 70:1628–1642.
- Hoyle, M., S. Kuyucak, and S. H. Chung. 1998. Computer simulation of ion conduction in membrane channels. *Phys. Rev. E.* (in press).
- Jakobsson, E., and S.-W. Chiu. 1987. Stochastic theory of singly occupied ion channels. *Biophys. J.* 52:33–46.
- Kuyucak, S., and S. H. Chung. 1994. Temperature dependence of conductivity in electrolyte solutions and ionic channels of biological membranes. *Biophys. Chem.* 52:15–24.
- Kuyucak, S., M. Hoyle, and S. H. Chung. 1998. Analytical solutions of Poisson's equation for realistic geometrical shapes of membrane ion channels. *Biophys. J.* 74:22–36.
- Li, S. C., M. Hoyle, S. Kuyucak, and S. H. Chung. 1998. Brownian dynamics study of ion transport in the vestibule of membrane channels. *Biophys. J.* 74:37–47.
- Milburn, T., D. A. Saint, and S. H. Chung. 1995. The conductance of the cardiac sodium channel: implications for mechanisms of ion permeation. *Receptors Channels.* 3:201–211.
- Pauling, L. 1942. *The Nature of the Chemical Bond*. Cornell University Press, Ithaca, NY.
- Press, W. H., B. P. Flannery, S. A. Teukolsky, and W. T. Vetterling. 1989. *Numerical Recipes*. Cambridge University Press, Cambridge.
- Rae, J. L., R. A. Levis, and R. S. Eisenberg. 1988. Ionic channels in ocular epithelia. In *Ion Channels*, Vol. 1. T. Narahashi, editor. Plenum Press, New York. 283–327.
- Reif, F. 1965. *Fundamentals of Statistical and Thermal Physics*. McGraw-Hill, Kogakusha, Tokyo.



- Roux, B., and M. Karplus. 1991a. Ion transport in a model gramicidin channel: structure and thermodynamics. *Biophys. J.* 59:961–981.
- Roux, B., and M. Karplus. 1991b. Ion transport in a gramicidin-like channel: dynamics and mobility. *J. Phys. Chem.* 95:4856–4868.
- Sansom, M. S. P., I. D. Kerr, J. Breed, and R. Sankaramakrishnan. 1996. Water in channel-like cavities: structure and dynamics. *Biophys. J.* 70:693–702.
- Sansom, M. S. P., G. R. Smith, C. Adcock, and P. C. Biggin. 1997. The dielectric properties of water within model transbilayer pores. *Biophys. J.* 73:2404–2415.
- Toyoshima, C., and N. Unwin. 1988. Ion channel of acetylcholine receptor reconstructed from images of postsynaptic membranes. *Nature.* 336:247–250.
- Unwin, N. 1989. The structure of ion channels in membranes of excitable cells. *Neuron.* 3:665–676.
- van Gunsteren, W. F., and H. J. C. Berendsen. 1982. Algorithms for Brownian dynamics. *Mol. Phys.* 45:637–647.
- van Gunsteren, W. F., H. J. C. Berendsen, and J. A. Rullmann. 1981. Stochastic dynamics for molecules with constraints: Brownian dynamics of *n*-alkanes. *Mol. Phys.* 44:69–95.